

PHYSICAL REVIEW LETTERS

VOLUME 26

31 MAY 1971

NUMBER 22

Resolved Structure in Fe $K\alpha$ X Rays Produced by 30-MeV Oxygen Ions*

D. Burch and Patrick Richard

Center for Nuclear Studies, University of Texas, Austin, Texas 78712

and

R. L. Blake

Department of Astronomy and Enrico Fermi Institute, University of Chicago, Chicago, Illinois 60637

(Received 14 April 1971)

The Fe $K\alpha$ x-ray spectrum produced by 30-MeV O^{5+} bombardment is found to consist of two major components which have been identified as $1s \rightarrow 2p$ transitions shifted 38 and 68 eV above the $K\alpha_{1,2}$ energy due primarily to one and two additional vacancies, respectively, in the $2p$ shell.

The production of x rays by heavy ions in the 1-MeV/amu energy range has been reported¹ in which a comparison was made between the $K\alpha$ and $K\beta$ spectra² of Ca through Zn as produced by 6-MeV protons and 15-MeV oxygen ions. Solid-state Si(Li) detectors were adequate to measure energy shifts of about 50 and 150 eV for $K\alpha$ and $K\beta$ lines, respectively, and to observe line broadening of the oxygen-produced x rays relative to proton-induced x rays. These observations were interpreted as resulting from multiple inner-shell ionization created during the oxygen-ion-atom collisions. Hartree-Fock-Slater (HFS) calculations were presented that showed that the centroid energies of the oxygen-induced x rays were consistent with ion configurations involving up to three L -shell vacancies along with a varying number of M -shell vacancies. The broadening observed was attributed to the distribution of strength among various ionic configurations consistent with these limits, and it was suggested that higher-resolution measurements might possibly separate these individual components. In this paper we report this resolution of structure in the Fe $K\alpha$ line produced by 30-MeV O^{5+} bombardment.

The measurements were performed with a sin-

gle-crystal Bragg spectrometer coupled directly to the target-chamber vacuum system at 90° from the incident oxygen-beam direction. The Fe K x rays entered the spectrometer through a Soller collimator which limited the horizontal divergence to $2.0'$ full width at half-maximum (FWHM). The x rays were then reflected in the horizontal plane by a LiF crystal with a measured rocking curve of $21''$ FWHM and detected by a thin NaI(Tl) crystal. The zero crystal angle was determined by measuring the reflection on either side of the primary x ray beam through the collimator. Full details of the spectrometer are given elsewhere.³ The crystal and detector angles were rotated manually and independently to scan the relevant range of Bragg angles, 28° to 29° , in steps of $30''$. The intrinsic reproducibility of the absolute angle setting is $\pm 5''$.

A $2\text{-}\mu\text{A}$ beam of 30-MeV O^{5+} was produced by the University of Texas tandem Van de Graaff accelerator, momentum analyzed, and focused onto the target by a quadrupole lens. The target was a rolled Fe foil 6 mg/cm^2 thick positioned at 45° with respect to the incident beam direction. Normalization of data at each angular setting was provided by integrating the transmitted oxygen beam for a fixed number of microcou-

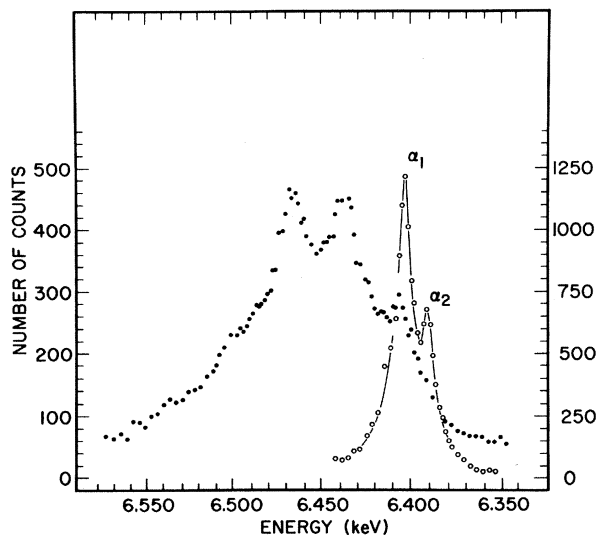


FIG. 1. Single-crystal spectrometer measurements of Fe $K\alpha$ x rays produced by 30-MeV oxygen-ion (solid circles) and 5-MeV proton (open circles) bombardments.

lombs.

In Fig. 1 are shown the Fe $K\alpha$ x-ray spectra as produced by 5-MeV protons and 30-MeV O^{5+} . The crystal d spacing and consequent absolute energy scale shown were determined by assuming that the proton-produced $K\alpha_1$ energy was identically the tabulated⁴ value of 6.4038 keV. From electron-beam measurements with this spectrometer and crystal, this is known to be true to ± 1 eV. The error is due primarily to the unmonitored crystal temperature difference between the proton and electron measurements. The resolution of the spectrometer on the Fe $K\alpha_1$ peak can be seen from the proton-induced line to be 6 eV FWHM. Higher-resolution (second-order) measurements were prohibited only by the lack of primary x-ray intensity. The background count rate in the NaI crystal (~ 0.1 count/sec) was not noticeably affected by the presence of the beam on target, therefore the peak-to-background ratio was limited only by the incident oxygen-beam intensity. Consequently, to reduce statistical fluctuations in the oxygen data, the spectrum was repeated several times, and the average of five runs is shown in the figure. This was not necessary for the proton measurements. The data show that the previously reported broadened peak¹ consists of two major components centered at 6.437 and 6.467 keV with some indication of structure at 6.500 keV along with a weak component at 6.405 keV which is only ~ 6 eV above the normal $K\alpha_{1,2}$ centroid energy.

Table I. HFS calculated energies for $1s \rightarrow 2p$ transitions with the indicated number of additional vacancies. These calculations are to be compared with the experimentally observed components centered at 6.437 and 6.467 keV. Also given are the HFS $K\beta/K\alpha$ intensity ratios for $(2p)^{-1}$ and $(2p)^{-2}$ configurations as a function of $3p$ vacancies.

L Shell		M Shell		X-Ray Energy (keV)	Intensity Ratio $K\beta/K\alpha$		
2s	2p	3p	3d				
1	1			6.422	0.136		
				6.430			
			1	6.432			
			1	6		6.429	
			1	2		6.435	
			1	2		6	6.433
			1	3		6.438	
			1	3		6	6.437
			1	4		6.442	
			1	5		6.445	
2	1			6.444	0.061		
				6.452			
			2	6.460			
			2	1		6.464	
			2	1		6	6.461
			2	2		6.467	
			2	2		6	6.465
			2	3		6.470	
			2	3		6	6.470
			2	4		6.474	
2	1			6.478	0.042		
				6.476			
			2	6.484			
			3	6.492			

As a first step in determining the origin of the peaks in Fig. 1, HFS calculations⁵ were performed as outlined in Ref. 1. The results of these calculations for Fe $K\alpha$ transitions with various L - and M -shell vacancies are given in Table I. As the present calculations do not distinguish between $K\alpha_1$ and $K\alpha_2$, the energies given represent the calculated shift added to the unshifted $K\alpha_{1,2}$ centroid energy. Some estimate of the reliability of the HFS $K\alpha$ -energy predictions can be made by a comparison to a full numerical integration of the Hartree-Fock equations. These latter calculations were carried out by Larkins⁶ for the following additional vacancy configurations in Fe: $(2p)^{-1}$, $(2p)^{-2}$, and $(2p)^{-3}$, with resulting predicted shifts in $K\alpha$ relative to $K\alpha_{1,2}$ of 29, 59, and 115 eV, respectively. These are to be compared to the HFS values of 30, 61, and 93 eV. This comparison lends some confidence to the identification by HFS calculations alone of the one- and two-vacancy energies.

It can be seen from Table I that the two major components correspond, approximately to the $K\alpha$ energies expected for Fe ions with one and two

holes, respectively, in the $2p$ shell. The measured difference in each case from these one- and two- $2p$ -vacancy calculations is 7 eV. If this difference is attributed to missing M -shell electrons, this would imply that, in addition to the $2p$ -shell vacancies, two to three additional $3p$ electrons are missing at the time of $K\alpha$ x-ray emission. Note from Table I that this conclusion is independent of the occupation of the $3d$ shell. The component at 6.405 keV is consistent with the $K\alpha$ energy with these two or three $3p$ vacancies alone. The unresolved structure at 6.500 keV is tentatively attributed to a $(2p)^{-3}$ configuration. Further evidence for this approximate number of $3p$ vacancies is given below.

The vacancies in the L shell responsible for the two major components of the observed $K\alpha$ spectrum can be identified as $2p$ rather than $2s$ for three reasons: (1) The HFS $K\alpha$ energies with additional $(2s)^{-1}$ and $(2s)^{-2}$ correspond to the positions of the two observed minima in the spectrum; (2) assuming that the number of subshell vacancies produced in the atom-ion collision is proportional to the number of electrons available, we would expect a 3-to-1 enhancement of $2p$ -shell-vacancy production; and (3) the existence of a large L_1 - $L_{23}M$ Coster-Kronig transition rate⁷ results in a rapid transfer of $2s$ vacancies to the $2p$ shell before a $1s \rightarrow 2p$ transition can occur.

In a similar manner the L_{23} - MM Auger transition which in turn transfers $2p$ vacancies to the

M shell also competes with the $1s \rightarrow 2p$ transition. It is thus evident that some comparison of these relative transition rates for defect configurations must be made. In Table II are presented the pertinent K and L single-vacancy transition rates and the estimated values of the modified transition rates for various defect configurations. These estimates were made by using the Slater screening rules⁸ to take into account the increase in the effective Z for a given shell due to the reduced screening in the defect configuration. The transition rates for the modified Z value are then determined graphically from a plot of calculated single-vacancy transition rates versus Z . A statistical weighting procedure⁹ has been used to take into account the reduction in the transition rates due to missing outer-shell electrons. For this analysis the following recent calculated values have been used for the unmodified transition rates: K and L radiative widths from Scofield,¹⁰ L_1 Auger and Coster-Kronig widths from McGuire,⁷ and L_2 and L_3 Auger and Coster-Kronig widths from Chen, Crasemann, and Kostroun.¹¹ We have neglected the L -shell radiative widths since they are ~ 100 times smaller than the non-radiative widths, and we have also neglected any possible influence of the two $4s$ electrons. The sum of the $K\alpha$ widths estimated in this manner agrees with HFS-calculated transition rates to within 5%, the calculated values being consistently but not systematically lower. The radiation-

Table II. Estimated Fe transition rates (eV/ \hbar) for various defect configurations.

K	L_1	L_2	L_3	M_1	M_{23}	M_{45}	K- L_2	K- L_3	L_1 -MM	L_1 - $L_{23}M$	L_2 -MM	L_2 - L_3M	L_3 -MM
1	1	1	1				0.120	0.234	0.348	7.30	1.292	0.101	1.321
1	1	1					0.127	0.248	0.352	7.65	1.305	0.120	
1		1	1				0.064	0.248					1.344
1			1				0.127	0.186					
1	2						0.135	0.263	0.410	7.80			
1		2						0.263			1.311	0.128	
1			2				0.135	0.132					1.353
1	1	1					0.067	0.197			1.311	0.128	1.353
1	1	1			2		0.067	0.197			0.950	0.109	0.980
1	1	1			4		0.067	0.197			0.648	0.091	0.669
1	1	1			6		0.067	0.197			0.403	0.073	0.416
1	1	1			1	6	0.067	0.197			0.302		0.312
1	1	1			2	6	0.067	0.197			0.216		0.223
1	1	1			3	6	0.067	0.197			0.144		0.148
1	1	1			4	6	0.067	0.197			0.086		0.089

less estimates are, of course, expected to be considerably less accurate. The tabulated results imply that at least eight M -shell vacancies are required to reduce the dominant transition tending to remove the L vacancies L_{23} - MM to the approximate value of the decreased K - L_3 width. This conclusion assumes that the L_{23} - MM rate is independent of the M subshells involved. Removing these eight progressively from the outer shells results in two $3p$ vacancies. In the other extreme, if the L_{23} - MM rate involves primarily only $3p$ electrons, then this analysis implies that three or four $3p$ electrons alone would be sufficient to reduce the L_{23} - MM rate by this amount. We therefore conclude that considerations of the competition between K - and L -shell transition rates require indirectly about two or three $3p$ -shell vacancies with no more detailed information concerning the $3d$ -shell occupation.

Another means of estimating the number of $3p$ vacancies relative to the number of $2p$ vacancies is to measure the ratio $K\beta/K\alpha$. Using a Si(Li) detector which is capable of resolving $K\alpha$ and $K\beta$ well, the Fe $K\beta_{1,3}/K\alpha_{1,2}$ ratio for 5-MeV incident protons is found to be 0.129 ± 0.005 . This value agrees with source measurements of 0.1283 ± 0.0025 .¹² Under identical experimental conditions, the 30-MeV O^{5+} incident beam results in a $K\beta/K\alpha$ ratio of 0.119 ± 0.005 . From the HFS calculations given in Table I we see that one and two vacancies in the $2p$ shell correspond to one or two and two or three vacancies, respectively, in the $3p$ shell. Additional information concerning the M -subshell occupation could be gotten from similar energy and intensity measurements of $K\beta$ and L x-ray spectra. Partial results of a systematic study of oxygen-ion-induced L x rays for $Z \geq 40$ have been reported.¹³

Because of the three independent, though indirect, estimates of two or three $3p$ vacancies, the observed $(2p)^{-1}$ component is very likely not simply an enhanced observation of the known Fe $K\alpha$ satellites.¹⁴ The most intense of these satellites, $K\alpha_3$ (6.431 keV) and $K\alpha_4$ (6.435 keV), have been identified as both originating from a $(2p)^{-1}$ configuration with no other additional vacancies. The 6.437-keV peak undoubtedly represents a similar transition in the presence of additional M -shell vacancies. The $(2p)^{-2}$ component reported here does not correspond to any known Fe satellite.

Several aspects of the possible influence of the target thickness on high-resolution measurements should be pointed out. From Si(Li) measurements ($\Delta E \sim 160$ eV FWHM) it is known¹⁵ that

the magnitude of the observed shift in the oxygen-induced x rays in the Fe region is dependent upon the incident ion energy. Beginning at ~ 500 keV (where no effect is observed) the shift slowly increases with energy up to the maximum energy studied, ~ 50 MeV. This would imply that the relative intensities of the various ion configurations produced are changing with incident energy. The energy loss for 30-MeV oxygen ions in 6 mg/cm² of Fe is ~ 25 MeV.¹⁶ The fact that the centroid energy reported here agrees with the Si(Li) predictions for 30 MeV reflects the influence of the very strong energy dependence of the x-ray yield. Measured cross sections for oxygen-ion x-ray production in the Fe region¹⁵ decrease ~ 4 orders of magnitude in the energy range of 30 to 10 MeV. Hence, the x rays observed are essentially those from the first layers of the target corresponding to a relatively small energy loss.

To summarize, we find that high-energy heavy-ion-atom collisions result in observable x rays which are *predominantly* from multiply ionized atoms. It appears promising that more detailed, higher-resolution measurements including systematic studies of Z dependence and incident energy dependence along with more exact atomic-structure calculations will make possible an improved specification of the ionic configuration at the time of x-ray emission. Measurements of this type would then allow for a self-consistent test of open-shell-configuration calculations; the experimental data which would be readily available for comparison are absolute energies, relative intensities, and the approximate limits set on the transition widths as outlined above. Studies of this type are essential for determining the number and location of the primary vacancies created during the atom-ion collision and a subsequent better understanding of the ionization process itself. Finally there is a rich field of application in solar x-ray spectroscopy where multiple defect configurations are involved in many x-ray flare events.¹⁷ $K\alpha$ transitions in Fe XX-Fe XXV have also recently been observed in a point plasma.¹⁸

The authors wish to thank D. McCrary and M. Senglaub for assistance with the experiment, and Dr. H. Wolter for providing us with a working version of the Herman-Skillman program.

*Work supported in part by the U. S. Atomic Energy Commission and the U. S. Air Force Office of Scientific Research.

¹D. Burch and P. Richard, Phys. Rev. Lett. 25, 983 (1970); P. Richard, I. L. Morgan, T. Furuta, and D. Burch, Phys. Rev. Lett. 23, 1009 (1969).

²The notation $K\alpha$ with no subscript on α is herein used to designate any $1s \rightarrow 2p$ transition independent of the number or orbitals of the other electrons. This is to be distinguished from, for example, $K\alpha_1$ which implies a distinct energy and an initial- and final-state configuration.

³R. L. Blake, thesis, University of Colorado, 1968 (unpublished).

⁴J. A. Bearden, Rev. Mod. Phys. 39, 78 (1967).

⁵F. Herman and S. Skillman, *Atomic Structure Calculations* (Prentice-Hall, Englewood Cliffs, N.J., 1963).

⁶F. P. Larkins, private communication.

⁷E. J. McGuire, Phys. Rev. A 3, 587 (1971).

⁸J. C. Slater, Phys. Rev. 36, 57 (1930).

⁹E. J. McGuire, Phys. Rev. 185, 1 (1969); F. P. Larkins, to be published.

¹⁰J. H. Scofield, Phys. Rev. 179, 9 (1969).

¹¹M. H. Chen, B. Crasemann, and V. O. Kostroun, to be published.

¹²J. S. Hansen, H. U. Freund, and R. W. Fink, Nucl. Phys. A 142, 604 (1970).

¹³D. Burch and P. Richard, Bull. Amer. Phys. Soc. 16, 74 (1971).

¹⁴L. G. Parratt, Phys. Rev. 50, 1 (1936); D. J. Candlin, Proc. Phys. Soc., London, Sect. A 68, 323 (1955).

¹⁵D. Burch and P. Richard, to be published.

¹⁶L. C. Northcliffe and R. F. Shilling, Nucl. Data, Sect. A 7, 233 (1970).

¹⁷R. L. Blake and L. L. House, to be published.

¹⁸T. H. Lie and R. C. Elton, Phys. Rev. A 3, 865 (1971).

Photoionization Cross Section of the Neutral Iron Atom*

Hugh Kelly and Akiva Ron†

Department of Physics, University of Virginia, Charlottesville, Virginia 22901

(Received 31 March 1971)

The photoionization cross section of the neutral iron atom is calculated from threshold at 7.90 eV to 36 eV. Results are presented for the Hartree-Fock approximation and correlations are included by many-body perturbation theory.

We have calculated the photoionization cross section $\sigma(\omega)$ of the neutral iron atom by means of the many-body perturbation theory of Brueckner¹ and Goldstone² and by our methods^{3,4} for evaluating the diagrams for atoms. This calculation was stimulated by its relevance for astrophysics⁵ and by the fact that there does not seem to be any measurement of $\sigma(\omega)$ for Fe.⁶ In these calculations we use the relation⁷

$$\sigma(\omega) = (4\pi/c)\omega \text{Im}\alpha(\omega), \quad (1)$$

where $\alpha(\omega)$ is the frequency-dependent polarizability.^{8,9} Atomic units are used throughout this paper unless otherwise indicated.

In calculating the perturbation-theory diagrams⁹ for $\alpha(\omega)$, we treat energy denominators according to the usual prescription $P-i\pi\delta$, where P represents a principal-value integration. Then $\text{Im}\alpha(\omega)$ consists of all diagrams in which we have an odd number of contributions from $-i\pi\delta$. The lowest-order diagram contributing to $\alpha(\omega)$ is shown in Fig. 1(a). The horizontal line represents use of $-i\pi\delta$. This notation has also been used by Wendin who has discussed calculation of resonances in $\sigma(\omega)$ by many-body theory.¹⁰ In Fig. 1, the heavy dot represents matrix elements

of z . [In calculating $\alpha(\omega)$ we take the perturbing electric field in the \hat{z} direction and average over M_L .] The dashed lines with no heavy dot represent Coulomb correlations. In the next order of perturbation theory there are diagrams as shown in Figs. 1(b) and 1(c). These diagrams also occur inverted and there are corresponding exchange diagrams. When there is no horizontal

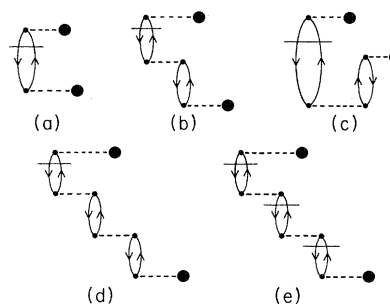


FIG. 1. Lowest-order diagrams contributing to the photoionization cross section or $\text{Im}\alpha(\omega)$. The horizontal line indicates a denominator contribution $-i\pi\delta$. The heavy dot indicates a matrix element of z . (a) Lowest-order diagram. (b), (c) Diagrams with one Coulomb interaction. These diagrams also occur inverted. The corresponding exchange diagrams should also be included. (d), (e) Higher-order diagrams.